Bias dependence of spin transfer torque in Co_2MnSi Heusler alloy based magnetic tunnel junctions

Cite as: Appl. Phys. Lett. **110**, 172403 (2017); https://doi.org/10.1063/1.4981388
Submitted: 18 January 2017 • Accepted: 06 April 2017 • Published Online: 26 April 2017

Jie Zhang, Timothy Phung, Aakash Pushp, et al.

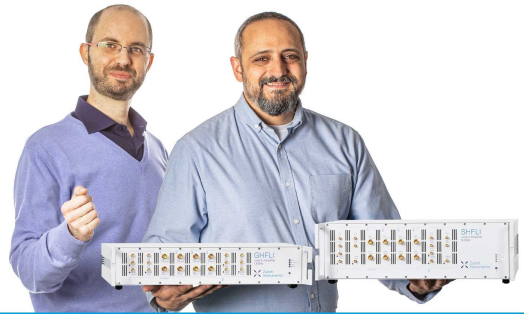

Bias dependence of spin transfer torque in Co_2MnSi Heusler alloy based magnetic tunnel junctions

Jie Zhang,[1,2] Timothy Phung,[2,a)] Aakash Pushp,[2] Yari Ferrante,[2] Jaewoo Jeong,[2] Charles Rettner,[2] Brian P. Hughes,[2] See-Hun Yang,[2] Yong Jiang,[1] and Stuart S. P. Parkin[2,3,a)]

[1]*School of Materials Science and Engineering, University of Science and Technology Beijing, Beijing 100083, China*

[2]*IBM Almaden Research Center, San Jose, California 95120, USA*

[3]*Max Planck Institute for Microstructure Physics, Halle (Saale) 06120, Germany*

(Received 18 January 2017; accepted 6 April 2017; published online 26 April 2017)

Heusler compounds are of interest as electrode materials for use in magnetic tunnel junctions (MTJs) due to their half metallic character, which leads to 100% spin polarization and high tunneling magnetoresistance. Most work to date has focused on the improvements to tunneling magnetoresistance that can stem from the use of Heusler electrodes, while there is much less work investigating the influence of Heusler electrodes on the spin transfer torque properties of MTJs. Here, we investigate the bias dependence of the anti-damping like and field-like spin transfer torque components in both symmetric (Co_2MnSi/MgO/Co_2MnSi) and asymmetric (Co_2MnSi/MgO/CoFe) structure Heusler based MTJs using spin transfer torque ferromagnetic resonance. We find that while the damping like torque is linear with respect to bias for both MTJ structures, the asymmetric MTJ structure has an additional linear component to the ordinarily quadratic field like torque bias dependence and that these results can be accounted for by a free electron tunneling model. Furthermore, our results suggest that the low damping and low saturation magnetization properties of Heusler alloys are more likely to lead significant improvements to spin torque switching efficiency rather than their half metallic character. *Published by AIP Publishing*. [http://dx.doi.org/10.1063/1.4981388]

Spin transfer torque Magnetic Random Access memory (STT-MRAM) is an emerging non-volatile memory technology that promises fast read and write times as well as essentially infinite endurance.[1–4] Information is encoded in STT-MRAM in the state of nano-scale magnetic elements that comprise a magnetic tunnel junction (MTJ). The state of the magnetic element is sensed using the tunneling magnetoresistance (TMR) effect,[5–8] while the writing process is based on using spin angular momentum transfer from spin-polarized electrical currents.[9–11] Currently, there is intense interest in investigating the physics and materials science of STT-MRAM devices for technological applications. One of the critical issues for technological viability of STT-MRAM is to reduce the current density required for switching the magnetic state of devices while maintaining high thermal stability of the magnetic elements. Moreover, one must have a sufficiently high TMR for readout of the magnetic state.

Recently, Heusler materials[12] have been proposed as electrode materials for MTJs due to their half metallic character, which is predicted to give rise to 100% spin polarization. Such large spin polarizations are thus expected to give rise to large TMR and also to increased switching efficiency.[13] Indeed, several reports have measured very high TMR in MTJs that are formed from Heusler materials.[14–18] However, there is much less work investigating the influence of the unique electronic structure of Heusler materials on the STT. Moreover, most studies of MTJs formed using Heusler electrodes involve free layers which are too thick (>5 nm) to investigate the STT switching phenomenon. In this letter, we use the spin torque ferromagnetic resonance (STFMR) technique to measure the bias dependence of the STT[19–21] in Heusler electrode based MTJs. Moreover, to date there have been only few demonstrations of the STT phenomenon in Heusler based MTJs.[22,23] One critical question to answer is the role of the presence of an energy gap in one of the spin sub-bands of a half-metallic Heusler compound in the STT phenomenon. It is thus crucial to develop a deep understanding of the STT in Heusler based electrode MTJs.

The films studied in this work are composed of the following layer structure (from bottom to top) 20 MgO | 400 Cr | core structure | 5 Ru | 25 $Co_{70}Fe_{30}$ | 150 $IrMn_3$ | 50 Ta | 50 Ru (where the thickness of each layer is in Angstroms) deposited on a MgO (001) substrate where the metallic layers were deposited by either DC magnetron sputtering (Heusler, $Co_{70}Fe_{30}$, and Ru) or ion beam sputtering (Cr, $IrMn_3$, and Ta) and the MgO layers deposited by radio-frequency (RF) magnetron sputtering. All the layers were grown at room temperature. One core structure, which we call the symmetric structure, consists of 20 Co_2MnSi | 9 MgO | 30 Co_2MnSi | 20 $Co_{70}Fe_{30}$ (CMS | MgO | CMS) and has a resistance area product (RA) of ~12 $\Omega\ \mu m^2$. The second core structure studied consists of 20 Co_2MnSi | 8 MgO | 20 $Co_{70}Fe_{30}$ (CMS | MgO | CoFe), referred to as the asymmetric structure and has a RA of 4 $\Omega \cdot \mu m^2$. The Cr and Co_2MnSi layers were deposited at room temperature and then annealed at 700 °C and 500 °C. We use Rutherford backscattering spectrometry (RBS) measurements to determine that the deposited CMS films have composition very close to 2:1:1 stoichiometry with Co, Mn, and Si atomic concentrations as 49.2 ± 2%, 26.8 ± 2%, and 24 ± 1%, respectively. Fig. 1(a) shows a high-resolution transmission

a)phungt@us.ibm.com and stuart.parkin@mpi-halle.mpg.de

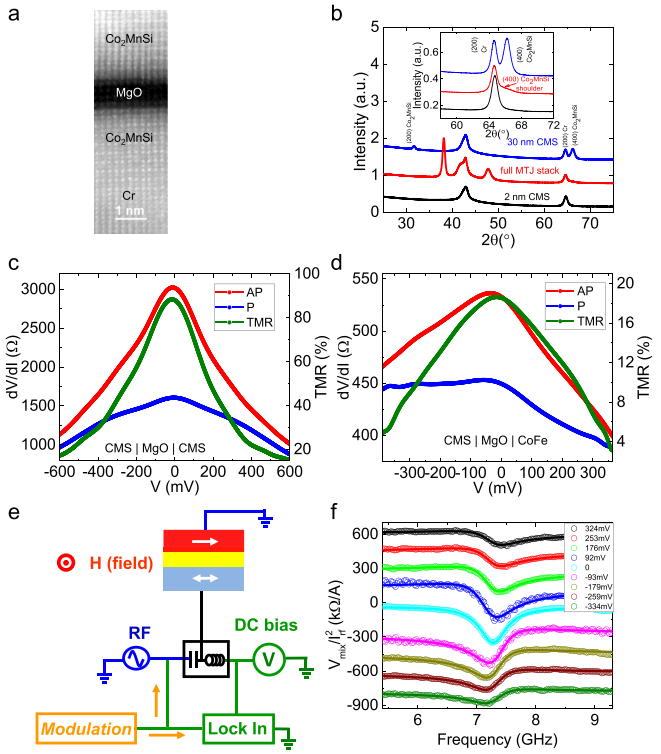

FIG. 1. (a) High resolution cross-section transmission electron micrograph (TEM) of the CMS | MgO | CMS device structure. (b) X-ray diffraction (XRD) patterns of a 2 nm CMS film, full CMS | MgO | CMS structure film, and a 30 nm thick CMS film deposited on MgO substrates with identical deposition procedures for each of the CMS layers. Differential resistances $\left(\frac{dV}{dI}\right)$ in anti-parallel (AP) (red) and parallel (P) (blue) state and tunneling magnetoresistance (TMR) (green) for (c) CMS | MgO | CMS and (d) CMS | MgO | CoFe structures. (e) Schematic diagram of the STFMR measurement circuit. (f) Representative bias voltage dependence of $\frac{V_{mix}}{I_{rf}^2}$ vs. frequency for a CMS | MgO | CMS MTJ device. Symbols are data and lines are fits to a Lorentzian function.

electron microscopy image taken of a cross-section of a representative device. The CMS layers show excellent epitaxy to both the Cr underlayer and the MgO layer. We note that there is very little Cr diffusion in the CMS layers as well. The free layer in each structure is a 20 Å thick Co_2MnSi (Heusler) layer. Both the reference and the free layer are patterned into rectangular cross sections. MTJs are patterned from the films by electron-beam lithography and Argon-ion milling into three to one aspect ratio sized devices, with the short axis of the device ranging from 50 nm to 150 nm. The devices shown in this paper are $50 \times 150\,nm^2$. Several devices of different sizes fabricated from the same film were measured and showed similar behavior. In our experiment, the voltage convention is defined such that positive bias corresponds to electrons flowing from the reference layer into the free layer. The experiments reported here are all performed at room temperature. X-ray diffraction (XRD) data are shown for a film stack comprising the free layer composed of (MgO substrate | 20 MgO | 400 Cr | 20 Co_2MnSi | 9 MgO | 50 Ta), a stack comprising a full MTJ stack (MgO substrate | 20 MgO | 400 Cr | 30 Co_2MnSi | 9 MgO | 30 Co_2MnSi | 20 $Co_{70}Fe_{30}$ | 150 $IrMn_3$ | 50 Ta | 50 Ru), and a stack similar to the free layer but with a 30 nm CMS layer (MgO substrate | 20 MgO | 400 Cr | 300 Co_2MnSi | 25 MgO | 50 Ta) (Fig. 1(b)). Clear peaks showing (200) and (400) oriented CMS are shown for the 30 nm thick CMS film. For films with much thinner (~2 nm) CMS layers, it is difficult to obtain sufficient XRD intensity, but the full MTJ stack shows evidence of a shoulder representing (400) oriented CMS. The patterned full MTJ stack also contains additional peaks corresponding to Au, Ru, and $IrMn_3$ layers (see Fig. S1 in the supplementary material for the complete annotated XRD pattern of this full MTJ stack). The Au layers are deposited to make contact to the MTJ devices. SQUID magnetometry (Fig. S2, supplementary material) on our films showed that the saturation magnetization to be 1089 emu/cm^3 and the effective magnetization to be 1050 emu/cm^3.

The MTJs exhibit square resistance (R) vs. magnetic field (H) minor loops with TMR of 88% in the CMS | MgO | CMS device and 19% in the CMS | MgO | CoFe device (Fig. S3, supplementary material). Figs. 1(c) and 1(d) show the bias dependence of differential resistance (dV/dI) in both parallel (P) and anti-parallel (AP) configurations of the devices, as well as the bias dependence of the TMR. We note that the change in dV/dI with respect to bias is more significant in the AP state compared to the P state. This behavior is similar to what has been observed in non-Heusler based MTJs and is commonly attributed to either the energy dependence of the density states of the electrode materials or energy-dependent transmission through the tunnel barrier.[24,25] At high bias, the excitation of magnons[26] can also reduce dV/dI. The TMR shows a dramatic decrease with voltage bias and becomes almost insignificant at high bias. At zero bias, the TMR value is 88% for the CMS | MgO | CMS device and then decreases to only 22% at 400 mV bias. By comparison, we note that dV/dI in both the AP and P states and the TMR decrease much less significantly with increasing bias for the CMS | MgO | CoFe device. Nevertheless, the CMS | MgO | CoFe displays a notable asymmetry in dV/dI as a function of the bias voltage polarity.

We use the STFMR technique to measure the STT components as a function of an applied bias voltage. Fig. 1(e) shows an illustration of the measurement circuit. This technique is based on the detection of a DC rectification voltage signal (V_{mix}) produced by an applied radio-frequency current (I_{rf}) and magnetoresistance signal that oscillates at the same frequency as I_{rf}. The magnetic field is applied in plane along the hard axis direction of the free layer of the MTJ in these experiments. Fig. 1(f) shows an example of representative signals that are observed with the addition of a DC bias voltage applied across the MTJ for the CMS | MgO | CMS device. The change in the lineshape of the resonance peak with respect to bias voltage can be utilized to obtain the bias dependence of the STT components. We utilize a flatness correction procedure that has been discussed in the literature[19] to account for the frequency (f) dependence of the applied RF current stemming from losses and standing waves along the cable. The spectra of V_{mix} that are obtained as a function of magnetic field and frequency of the RF current are shown in Figs. 2(a) and 2(b) for the symmetric and asymmetric stacks, respectively. Line cuts of V_{mix}/I_{rf}^2 are shown for selected H values in Figs. 2(c) and 2(d). There is a dominant peak that represents the quasi-uniform mode of oscillation of the free layer. The other peaks with significantly smaller signals correspond to edge modes or higher order spatially non-

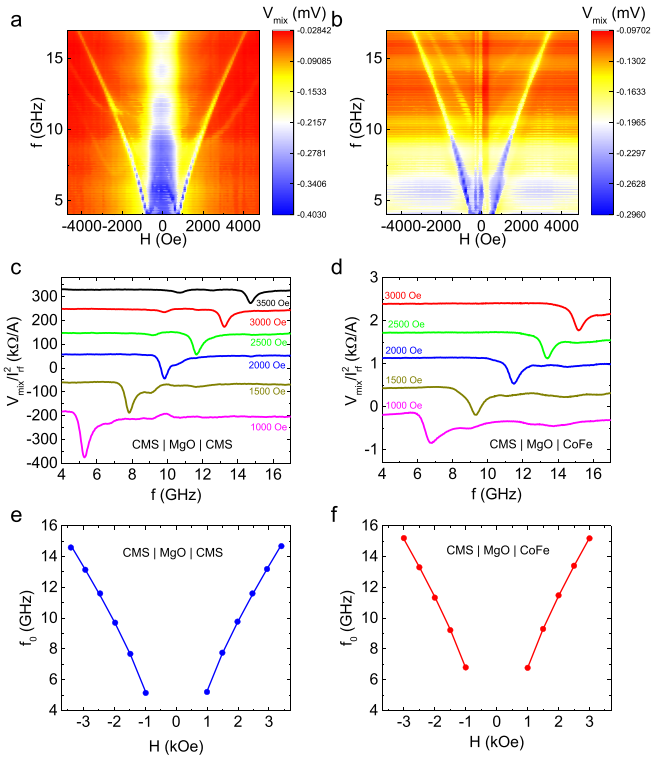

FIG. 2. Spectra of V_{mix} vs. frequency and magnetic field for (a) CMS | MgO | CMS and (b) CMS | MgO | CoFe structures. Line cuts of $\frac{V_{mix}}{I_{rf}^2}$ vs. frequency at certain magnetic field values for (c) CMS | MgO | CMS and (d) CMS | MgO | CoFe structures. Resonant frequency f_0 vs. magnetic field (symbols) and fitting to the Kittel formula (line) for (e) CMS | MgO | CMS and (f) CMS | MgO | CoFe structures.

uniform modes that are formed from coupled modes of the free layer and the fixed layer or from standing wave modes.[27,28] The resonant frequency (f_0) of these dominant modes can be plotted as a function of magnetic field, as shown in Figs. 2(e) and 2(f). By fitting to the Kittel equation, we obtain an effective magnetization M_{eff} value of the free layer of 492 emu/cm^3. The M_{eff} that we measure is significantly smaller than that determined by out of plane vibrating sample magnetometry measurements of blanket films of 1050 emu/cm^3. This is consistent with previous reports of ferromagnetic resonance performed on in-plane magnetized MTJs with magnetic field applied in plane and in the hard-axis direction of the MTJ free layer and is commonly attributed to patterning induced defects and dipolar coupling between the different MTJ layers.[28–30] Indeed, the difference in the resonant frequency for a given magnetic field in both MTJ stacks is due the different dipolar coupling between the reference and free layers since the reference layer for both stacks is not identical.

The V_{mix} signal that we measure can be decomposed into symmetric and asymmetric components, as is described by the following equation:[19] $V_{mix} = \frac{1}{4}\frac{\partial^2 V}{\partial I^2} {I_{rf}}^2 + \frac{1}{2}\frac{\partial^2 V}{\partial I \partial \theta}\frac{\hbar \gamma_0 \sin\theta}{4eM_s V 2\pi\Delta} I_{rf}^2[SF_s(f) - A\Omega F_A(f)]$, where $\hbar$ is Planck's constant, γ_0 is the gyromagnetic ratio, θ is the angle between the magnetization of the two layers that are separated by the tunnel barrier (namely, the free layer and the bottom most layer of the reference layer), M_s is the saturation magnetization of the free layer, V is the volume of the magnetic free layer, e is the electron charge, and Δ is the linewidth of the resonance. The first term of the equation is a rectification voltage that is produced by the non-linearity $(\frac{\partial^2 V}{\partial I^2})$ of the MTJ current (I)–voltage (V) characteristics and is used to calibrate the RF current I_{rf} running through the device. The second term is composed of symmetric and asymmetric Lorentzian functions, given by $F_s(f) = \frac{1}{1+\left(\frac{f-f_0}{\Delta}\right)^2}$ and $F_A(f) = \frac{(f-f_0)}{\Delta}F_s(f)$, where $\Omega = \gamma_0 (4\pi M_{eff} + H)/2\pi f_0$. The coefficients of the symmetric and asymmetric Lorentzian functions, S and A, respectively, are related to the so-called damping like $\left(\frac{d\tau_{||}}{dV}\right)$ and field like $\left(\frac{d\tau_{\perp}}{dV}\right)$ torkances by the following relations $\frac{d\tau_{||}}{dV} = \frac{\hbar \sin\theta}{2e}\frac{S}{\left(\frac{dV}{dI}\right)}$, and $\frac{d\tau_{\perp}}{dV} = \frac{\hbar \sin\theta}{2e}\frac{A}{\left(\frac{dV}{dI}\right)}$. Figs. 3(a)–3(d) show the torkance as well as the differential torques $\frac{d\tau_{||}}{dI}$ and $\frac{d\tau_{\perp}}{dI}$ derived based on using the formalism. The torkances can further be integrated in order to obtain the full bias dependence of the individual torque components which are shown in Figs. 3(e) and 3(f). For the symmetric device (blue triangles), the damping like torque $(\tau_{||})$ at low bias is linear with respect to bias voltage, with an enhancement at high bias due to heating, while the field like torque $(\tau_{\perp})$ shows a quadratic bias dependence. The bias dependence of this symmetric Heusler electrode based device is thus consistent with conventional symmetric ferromagnetic electrode based MTJ structures that have been studied both experimentally[19,20] and theoretically.[31] In the asymmetric structure device (red triangles), we find a linear bias dependence in the damping like torque as well, but on the contrary to the symmetric device, there is an additional linear

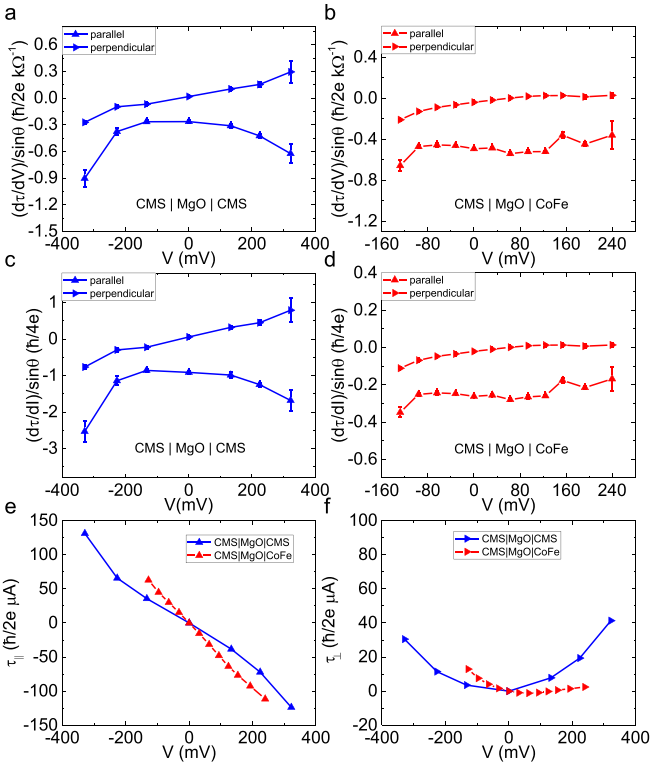

FIG. 3. Bias dependence of torkances $\frac{\frac{d\tau}{dV}}{\sin(\theta)}$ for parallel and perpendicular components of STT for (a) CMS | MgO | CMS and (b) CMS | MgO | CoFe structures. Differential torques $\frac{\frac{d\tau}{dI}}{\sin(\theta)}$ vs. bias voltage (V) for (c) CMS | MgO | CMS and (d) CMS | MgO | CoFe structures. Bias dependence of the STT components for CMS | MgO | CMS structure (blue) and CMS | MgO | CoFe structure (red) for (e) parallel component $\tau_{||}$ and (f) perpendicular component $\tau_{\perp}$.

component to the bias dependence of the field like torque on top of the quadratic component (see Fig. 3(f)). The Gilbert damping of our electrodes can also be attained using our ST-FMR data given by $\alpha = 2\Delta/(f_0(\Omega + \Omega^{-1})$. We find that the Gilbert damping for the CMS layers in our devices is given by 0.0166 ± 0.0005 and is comparable to that of polycrystalline Co_2FeAl at similar thicknesses (by comparison, the Gilbert damping is given by 0.0018 ± 0.00015 for a 30 nm thickness CMS film that is deposited by the same procedure (Fig. S4, supplementary material)).

To understand our results, we use a model that has been proposed by Manchon *et al.*[32] that can be used to calculate the bias dependence of both STT components and the conductance. The model, which is schematically illustrated in Fig. 4(a) for the generic case of a MTJ with asymmetric electrodes, treats both magnetic electrodes of the MTJ with spin-split free electron dispersion relations (Fig. 4(a)). Each electrode is modeled as having an exchange splitting J_i and workfunction ϕ_i, where $i = L, R$ for the left and right electrodes, respectively. We model the Co_2MnSi electrodes by considering them to be close to the half-metallic limit. The Fermi-level is at 2.25 eV whereas the exchange splitting[14] is taken to be J = 2.05 eV. The work function for this electrode is 3.55 eV based on literature values.[33] The thickness of the tunnel barrier is chosen to be 8 Å. The CoFe layer is simulated by considering an exchange splitting[25] of 1.75 eV and work function[34] of 4.75 eV. Using such a model (Figs. 4(b)–4(d)), the salient features of our experimental data can be accounted for in the observed torque bias dependence as well as for the differential resistance bias dependence. The torques are plotted in normalized form as follows: the parallel component of the torque is normalized to the torkance value at zero bias voltage of the CMS | MgO | CMS structure, while the perpendicular torque is normalized to the perpendicular torque value at zero bias. The differential resistances are normalized to the differential resistances in the parallel state at zero bias. We find that the main observed features in the asymmetric structure data can be accounted for by considering only the differences in the exchange coupling of both magnetic electrodes. The work function difference can account for the observed conductance variation, but it actually predicts trends in the field like torque that are opposite to what we observe. This implies that the experimental trends we observe most likely arise due to the change in the relative band filling of the majority and minority spin sub-bands in both the symmetric and asymmetric structures, rather than due to the work function changes in the band structure of the Co_2MnSi and CoFe electrodes. While our model considers the electrodes to be close the half-metallic limit, we have also performed a model with fully half metallic electrodes and find the similar trends (Fig. S5, supplementary material).

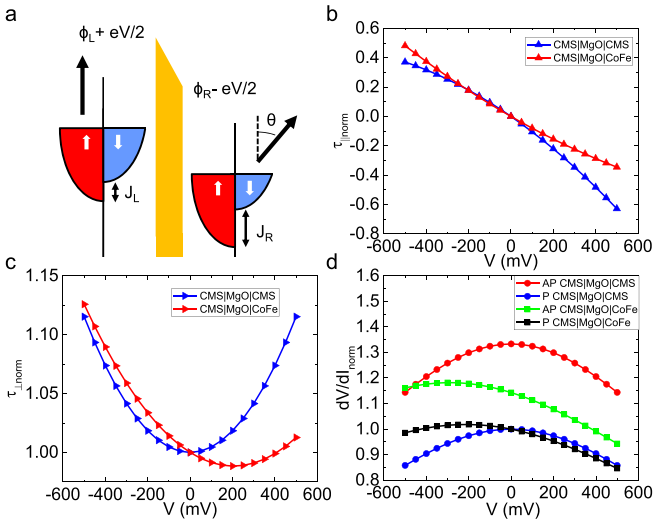

FIG. 4. (a) Schematic of the free-electron dispersion based tunneling model used for calculating the bias dependence of the STT and the differential resistance. The electrodes, each have an exchange splitting J_i and workfunction ϕ_i, where $i = L, R$ for the left and right electrodes, respectively. The arrows denote the magnetization of both layers. Bias dependence of normalized (b) parallel and (c) perpendicular STT components calculated based on free electron tunneling model. (d) Normalized differential resistance dV/dI in anti-parallel (AP) (red) and parallel (P) (blue) states for the CMS | MgO | CMS structure and dV/dI in anti-parallel (AP) (green) and parallel (P) (black) states for the CMS | MgO | CoFe structure calculated based on the model.

It is also useful to examine the torque per unit electron that we obtain in our MTJs, which is given by the differential torques in Figs. 3(c) and 3(d) and to compare predictions from an elastic tunneling model. For the symmetric device, we find a torque per unit electron of $(0.91 \pm 0.05)\frac{\hbar}{4}\sin(\theta)$. Based on the TMR value of 88%, we expect a polarization $P = 0.55$ based on using the Julliere model[35] and hence a torque per unit electron of $0.85\ \frac{\hbar}{4}\sin(\theta)$. Moreover, even in the case we could develop a perfect half-metallic electrode, i.e., fully spin-polarized ($P = 1$), the value of the torque per unit electron in the latter case would only change to $\frac{\hbar}{4}\sin(\theta)$. This implies that the torque per unit electron in our material under study is already close to this maximum value. We surmise that this is due to the excellent spin filtering properties of the MgO barrier[5,6] as Heusler electrodes such as CMS have very little lattice mismatch to MgO.[12] Indeed, standard CoFeB electrodes interfaced with MgO are also already very close to the ideal case.[19] Nevertheless, for technological applications, one can still improve the STT efficiency using Heusler materials, by studying their low saturation magnetization values and low Gilbert damping.[12] In particular, the half metallic properties of Heusler compounds can still improve MTJ switching efficiency through suppression of the interband scattering contribution of the Gilbert damping.[36,37] Moreover, the high spin polarization of MTJs using Heusler electrodes will also be useful in improving the TMR. Additionally, consistent with conventional ferromagnetic metal based MTJs, we find that the STT stays finite and large even when the TMR is suppressed with bias voltage.

In summary, we have measured the bias dependent STT components in both CMS | MgO | CMS and CMS| MgO | CoFe based MTJ structures and have correlated our results to a free-electron model, which can account for the experimental data. Our findings show that for the symmetric MTJ structure, the damping like torque displays a linear bias dependence and the field like torque shows a quadratic bias dependence. This is consistent with what is also typically observed in symmetric MTJ structures made with standard ferromagnetic (i.e., CoFeB) electrodes. Instead in the asymmetric structure, the field like torque is asymmetric with

respect to the bias voltage and contains an additional linear component on top of the quadratic dependence that is usually observed in the symmetric MTJ structure. Lastly, we find that, in the context of STT-MRAM, the half-metallic character of the Heusler electrodes is likely to be more beneficial for improving the TMR and that the low saturation magnetization and damping of Heusler compounds are the intrinsic properties that will be more useful in order to reduce the current densities required for STT driven magnetization reversal.

See supplementary material for an annotated XRD pattern of the patterned full MTJ stack, magnetization characterization measurements, representative easy axis RH-loops of the devices considered, stripline FMR data of the 30 nm CMS film, and theoretical modeling of the STT and differential conductance in the fully half metallic limit.

We thank J. Z. Sun, K. P. Roche, X. Jiang, and P. Filippou for fruitful discussions, and A. Kellock for RBS measurements, and E. A. Delenia and T. Topuria for high resolution TEM. The work of J. Zhang was partially supported through China Scholarship Council.

[1]D. Apalkov, B. Dieny, and J. M. Slaughter, Proc. IEEE **104**, 1796 (2016).
[2]A. D. Kent and D. C. Worledge, Nat. Nanotechnol. **10**, 187 (2015).
[3]S. Ikeda, K. Miura, H. Yamamoto, K. Mizunuma, H. D. Gan, M. Endo, S. Kanai, J. Hayakawa, F. Matsukura, and H. Ohno, Nat. Mater. **9**, 721 (2010).
[4]D. C. Worledge, G. Hu, D. W. Abraham, J. Z. Sun, P. L. Trouilloud, J. Nowak, S. Brown, M. C. Gaidis, E. J. O'Sullivan, and R. P. Robertazzi, Appl. Phys. Lett. **98**, 22501 (2011).
[5]W. Butler, X.-G. Zhang, T. Schulthess, and J. MacLaren, Phys. Rev. B **63**, 054416 (2001).
[6]J. Mathon and A. Umerski, Phys. Rev. B **63**, 220403 (2001).
[7]S. Yuasa, T. Nagahama, A. Fukushima, Y. Suzuki, and K. Ando, Nat. Mater. **3**, 868 (2004).
[8]S. S. P. Parkin, C. Kaiser, A. Panchula, P. M. Rice, B. Hughes, M. Samant, and S.-H. Yang, Nat. Mater. **3**, 862 (2004).
[9]J. C. Slonczewski, J. Magn. Magn. Mater. **159**, L1 (1996).
[10]L. Berger, Phys. Rev. B **54**, 9353 (1996).
[11]D. C. Ralph and M. D. Stiles, J. Magn. Magn. Mater. **320**, 1190 (2008).
[12]T. Graf, C. Felser, and S. S. P. Parkin, Prog. Solid State Chem. **39**, 1 (2011).
[13]J. C. Slonczewski and J. Z. Sun, J. Magn. Magn. Mater. **310**, 169 (2007).
[14]Y. Sakuraba, M. Hattori, M. Oogane, Y. Ando, H. Kato, A. Sakuma, T. Miyazaki, and H. Kubota, Appl. Phys. Lett. **88**, 192508 (2006).
[15]S. Tsunegi, Y. Sakuraba, M. Oogane, K. Takanashi, and Y. Ando, Appl. Phys. Lett. **93**, 112506 (2008).
[16]W. Wang, H. Sukegawa, R. Shan, S. Mitani, and K. Inomata, Appl. Phys. Lett. **95**, 182502 (2009).
[17]N. Tezuka, N. Ikeda, F. Mitsuhashi, and S. Sugimoto, Appl. Phys. Lett. **94**, 162504 (2009).
[18]H. Liu, Y. Honda, T. Taira, K. Matsuda, M. Arita, T. Uemura, and M. Yamamoto, Appl. Phys. Lett. **101**, 132418 (2012).
[19]J. C. Sankey, Y.-T. Cui, J. Z. Sun, J. C. Slonczewski, R. A. Buhrman, and D. C. Ralph, Nat. Phys. **4**, 67 (2008).
[20]H. Kubota, A. Fukushima, K. Yakushiji, T. Nagahama, S. Yuasa, K. Ando, H. Maehara, Y. Nagamine, K. Tsunekawa, D. D. Djayaprawira, N. Watanabe, and Y. Suzuki, Nat. Phys. **4**, 37 (2008).
[21]A. A. Tulapurkar, Y. Suzuki, A. Fukushima, H. Kubota, H. Maehara, K. Tsunekawa, D. D. Djayaprawira, N. Watanabe, and S. Yuasa, Nature **438**, 339 (2005).
[22]H. Sukegawa, Z. Wen, K. Kondou, S. Kasai, S. Mitani, and K. Inomata, Appl. Phys. Lett. **100**, 182403 (2012).
[23]Z. Wen, H. Sukegawa, S. Kasai, K. Inomata, and S. Mitani, Phys. Rev. Appl. **2**, 24009 (2014).
[24]M. Sharma, S. Wang, and J. Nickel, Phys. Rev. Lett. **82**, 616 (1999).
[25]S. O. Valenzuela, D. J. Monsma, C. M. Marcus, V. Narayanamurti, and M. Tinkham, Phys. Rev. Lett. **94**, 196601 (2005).
[26]S. Zhang, P. Levy, A. Marley, and S. Parkin, Phys. Rev. Lett. **79**, 3744 (1997).
[27]R. D. McMichael and M. D. Stiles, J. Appl. Phys. **97**, 10J901 (2005).
[28]Z. Zeng, K. H. Cheung, H. W. Jiang, I. N. Krivorotov, J. A. Katine, V. Tiberkevich, and A. Slavin, Phys. Rev. B: Condens. Matter Mater. Phys. **82**, 100410(R) (2010).
[29]S. Petit, N. De Mestier, C. Baraduc, C. Thirion, Y. Liu, M. Li, P. Wang, and B. Dieny, Phys. Rev. B: Condens. Matter Mater. Phys. **78**, 184420 (2008).
[30]S. Cornelissen, L. Bianchini, A. Helmer, T. Devolder, J. Von Kim, M. Op De Beeck, W. Van Roy, L. Lagae, and C. Chappert, J. Appl. Phys. **105**, 07B903 (2009).
[31]I. Theodonis, N. Kioussis, A. Kalitsov, M. Chshiev, and W. H. Butler, Phys. Rev. Lett. **97**, 237205 (2006).
[32]A. Manchon, S. Zhang, and K. J. Lee, Phys. Rev. B: Condens. Matter Mater. Phys. **82**, 174420 (2010).
[33]R. Fetzer, J. P. Wüstenberg, T. Taira, T. Uemura, M. Yamamoto, M. Aeschlimann, and M. Cinchetti, Phys. Rev. B: Condens. Matter Mater. Phys. **87**, 184418 (2013).
[34]K. R. Jeon, B. C. Min, Y. H. Jo, H. S. Lee, I. J. Shin, C. Y. Park, S. Y. Park, and S. C. Shin, Phys. Rev. B **84**, 165315 (2011).
[35]M. Julliere, Phys. Lett. A **54**, 225 (1975).
[36]M. Oogane and S. Mizukami, Philos. Trans. R. Soc., A **369**, 3037 (2011).
[37]C. Liu, C. K. A. Mewes, M. Chshiev, T. Mewes, and W. H. Butler, Appl. Phys. Lett. **95**, 22509 (2009).